Soft Matter

Cite this: *Soft Matter*, 2012, **8**, 6445

www.rsc.org/softmatter

PAPER

Nanogel formation of polymer solutions flowing through porous media

Laura Campo-Deaño,*[a] Francisco J. Galindo-Rosales,[a] Fernando T. Pinho,[a] Manuel A. Alves[a] and Mónica S. N. Oliveira[ab]

Received 21st March 2012, Accepted 26th April 2012
DOI: 10.1039/c2sm25654a

A gelation process was seen to occur when Boger fluids made from aqueous solutions of polyacrylamide (PAA) and NaCl flowed through porous media with certain characteristics. As these viscoelastic fluids flow through a porous medium, the pressure drop across the bed varies linearly with the flow rate, as also happens with Newtonian fluids. Above a critical flow rate, elastic effects set in and the pressure drop grows above the low-flow-rate linear regime. Increasing further the flow rate, a more dramatic increase in the slope of the pressure drop curve can be observed as a consequence of nanogel formation. In this work, we discuss the reasons for this gelation process based on our measurements using porous media of different sizes, porosity and chemical composition. Additionally, the rheological properties of the fluids were investigated for shear and extensional flows. The fluids were also tested as they flowed through different microfluidic analogues of the porous media. The results indicate that the nanogel inception occurs with the adsorption of PAA molecules on the surface of the porous media particles that contain silica on their surfaces. Subsequently, if the interparticle space is small enough a jamming process occurs leading to flow-induced gel formation.

1 Introduction

A porous medium consists of a solid material permeated by a network of interconnected pores, or voids.[1] In the last few years, various studies dealing with the flow of non-Newtonian fluids through porous media have been carried out.[2–4] The importance of porous media flows lies in the wide range of engineering applications, particularly in areas such as crude oil recovery, filtration of suspensions in polymer solutions and flow in soils.[2]

One of the reasons for the complexity of the flow in porous media, is that it is neither a pure shear nor a pure elongational flow, but a complex combination of both, with a strong shear component near the particle walls and a strong extensional component away from the walls due to the converging–diverging flow paths.[5] For non-Newtonian fluids there is an added degree of complexity as the flow may combine inertial and elastic nonlinearities.[6]

Dilute aqueous polyacrylamide (PAA) solutions are used frequently in enhanced oil recovery applications[7,8] and in microfluidic research in the formulation of viscoelastic fluids with constant shear viscosity, also known as Boger fluids.[9–12] The use of Boger fluids in porous media devices is very convenient due to their shear-independent viscosity, allowing the analysis of elastic behaviour isolated from other non-linear effects. As such, changes in the flow kinematics relative to those of Newtonian fluids can undoubtedly be associated with fluid elasticity.

Different porous media analogue devices, at the micro- and macro-scale, have been developed over the years,[1,6,13,14] in order to investigate the effect of fluid flow elasticity and to study multiphase transport in porous media. However, so far there are still many unanswered questions regarding these phenomena, such as flow-induced structure formation in a microporous flow,[15] adsorption of polymers on walls, mechanical retention and pore blockage,[5] all of which are difficult to replicate in the simplified analogues.

When low viscosity Boger fluids flow through a porous medium at low flow rates, the pressure drop is proportional to the flow rate, as also happens with Newtonian fluids. However, at higher flow rates there is an increase in the slope of the pressure gradient curve, induced by elastic effects.[6] On further increasing the flow rate, we found that the pressure gradient increases dramatically, most likely as a consequence of a blockage of the porous network, which we anticipate to be due to gel formation of the polymer solution. In the present work we envision to understand the causes for flow induced gel formation when low viscosity Boger fluids flow through porous media. To this end, various shear and extensional flow experiments were carried out for conditions that generate large shear and extensional deformation rates: (i) LAOS (large amplitude oscillatory shear) and steady-shear flow tests were performed to measure the rheological properties at high shear rates;[16,17] (ii) flow visualizations using microchannels with a hyperbolic contraction, which

[a]*CEFT, Faculdade de Engenharia da Universidade do Porto, Rua Dr Roberto Frias, 4200-465 Porto, Portugal. E-mail: campo@fe.up.pt; laura@campodeano.com; Fax: +351 22 508 1440; Tel: +351 22 508 1079*
[b]*Department of Mechanical and Aerospace Engineering, University of Strathclyde, Glasgow, G1 1XJ, United Kingdom*

induces a quasi-uniform extensional rate at the centre line of the microgeometry[12,18] were carried out to investigate the effects of the high extensional strain rates; (iii) the flow through various microchannel analogues of porous media was analyzed with the aim of reproducing the flow conditions leading to the gel formation observed in real porous media. The optical access to the flow in these types of devices allows us to visualize the flow patterns under controlled flow conditions, in contrast with the inherent limitations when real porous media are used.

2 Materials and methods

2.1 Fluid preparation

Polyacrylamide with a large average molecular weight ($M_w = 18 \times 10^6$ g mol^{-1}, Polysciences) was used to prepare the viscoelastic solutions by mixing the polymer into the solvent (de-ionized water) at different concentrations (50 and 125 ppm w/w) with 1% of NaCl (w/w), using magnetic stirrers at low speeds to prevent mechanical degradation of the polymer molecules. The detailed procedure for fluid preparation can be found in Campo-Deaño *et al.*[12]

2.2 Fluid rheology

Rheological characterization in shear flow was performed on a stress-controlled rotational rheometer (Anton Paar, model Physica MCR301), with a plate-plate geometry of 50 mm diameter and using a gap of 100 μm. Steady shear flow measurements in the range of shear rates, $0.1 \leq \dot{\gamma}/s^{-1} \leq 10000$, were carried out at 20.0 °C. As shown in Fig. 1a, both PAA solutions exhibit a nearly constant viscosity across the range of shear-rates tested (Boger fluid behaviour). The viscosities are 1.05 and 1.00 mPa s at high shear-rates for the more concentrated and less concentrated polymer solutions, respectively. LAOS experiments were also performed in order to evaluate the progressive transition from a linear to nonlinear rheological response and, simultaneously, to assess whether a simple shear flow at high shear rates can lead to shear induced gelation. These results are shown in Fig. 1b and will be discussed in section 3.2.2. In addition, the longest relaxation times were measured using a Capillary Breakup Extensional Rheometer (CaBER®) yielding $\lambda = 10$ and 4 ms for the 125 and 50 ppm solutions, respectively.

2.3 SEM and Cryo-SEM imaging

A scanning electron microscope (SEM) FEG-ESEM/EDS/EBSD (FEI Quanta 400FEG ESEM/EDAX Genesis X4M) and a Cryo-Scanning Electron Microscope FE-CryoSEM/EDS (JEOL JSM 6301F/Oxford INCA Energy 350/Gatan Alto 2500) were used for imaging the microchannels, the porous media particles, and the free and fractured surfaces of liquid nitrogen frozen fixed samples of porous media containing the PAA hydrogel formed in some porous media.

2.4 Porous media

Each of the real porous media used in this work consists of a hollow acrylic cylindrical tube (1.95 cm inner diameter) filled with an unconsolidated packed bed. The experimental set-up is similar to that used by Galindo-Rosales *et al.*[6] but in this work we employ a variety of unconsolidated beds with particles of different materials and different Sauter mean diameters, x_{32}: sand with $x_{32} = 400$ μm, glass beads (ballotini) with $x_{32} = 403$ μm and $x_{32} = 150$ μm, and plastic beads with $x_{32} = 142$ μm and

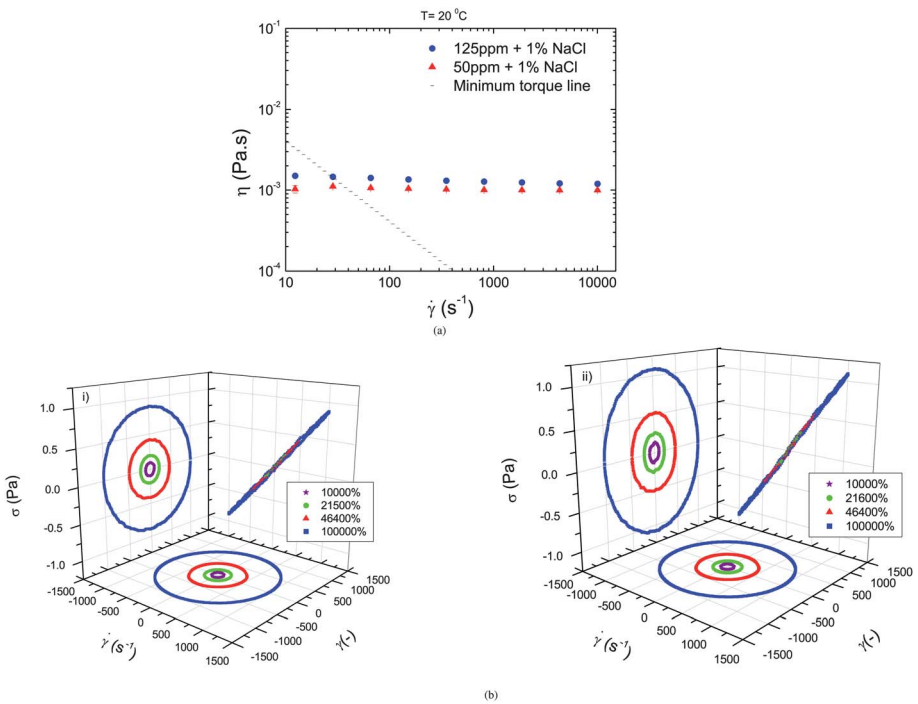

Fig. 1 Shear rheology experiments of 50 and 125 ppm PAA aqueous solutions with 1% of NaCl: (a) viscosity curve; (b) LAOS response at $\omega = 1$ rad s^{-1} and at different strains for (i) 50 ppm of PAA with 1% of NaCl, and (ii) 125 ppm of PAA with 1% of NaCl.

$x_{32} = 81$ μm. The Sauter mean diameters were calculated from the particle size distributions measured using a laser diffraction particle size analyser (Beckman Coulter LS 230). Fig. 2 shows the SEM images of the particles used. The particles of sand and ballotini with $x_{32} = 150$ μm display significant variations in size and shape, unlike the ballotini with $x_{32} = 403$ μm and the two types of plastic beads, for which the particle sizes are rather homogeneous and exhibit a spherical shape.

2.5 Microchannels, porous media analogues and flow visualization

Different microchannel configurations were used to investigate the flow characteristics under different flow types (shear dominated; extension dominated; mixed kinematics). The microchannels were fabricated in polydimethylsiloxane (PDMS) using standard soft-lithography techniques and SU-8 photo-resist moulds.

The microchannels used to observe the flow patterns at high elongational strain rates with a reduced influence of shear, are planar and present a single hyperbolic contraction followed by an abrupt expansion (Fig. 3a). The maximum width of the channel is $D_1 = 400$ μm, the minimum width of the contraction is $D_2 = 54$ μm and the length of the hyperbolic contraction is $L_c = 128$ μm, resulting in a total Hencky strain of $\varepsilon_H = \ln(D_1/D_2) = 2$.[12] The depth of the microchannel is constant, $h = 45$ μm.

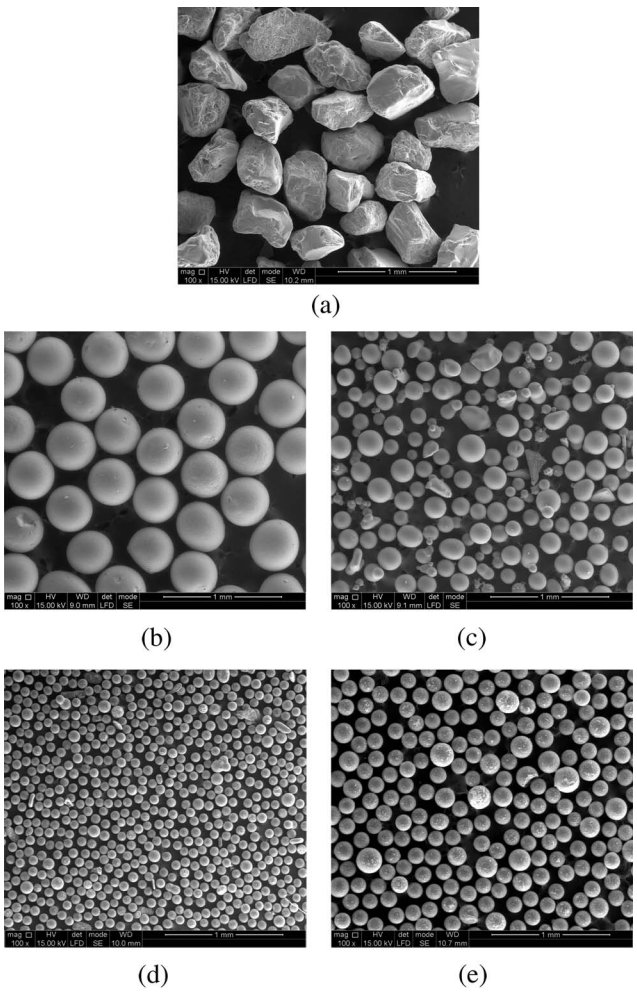

Fig. 2 SEM images: (a) sand of $x_{32} = 400$ μm; (b) ballotini of $x_{32} = 403$ μm and (c) $x_{32} = 150$ μm; (d) plastic beads of $x_{32} = 81$ μm and (e) $x_{32} = 142$ μm.

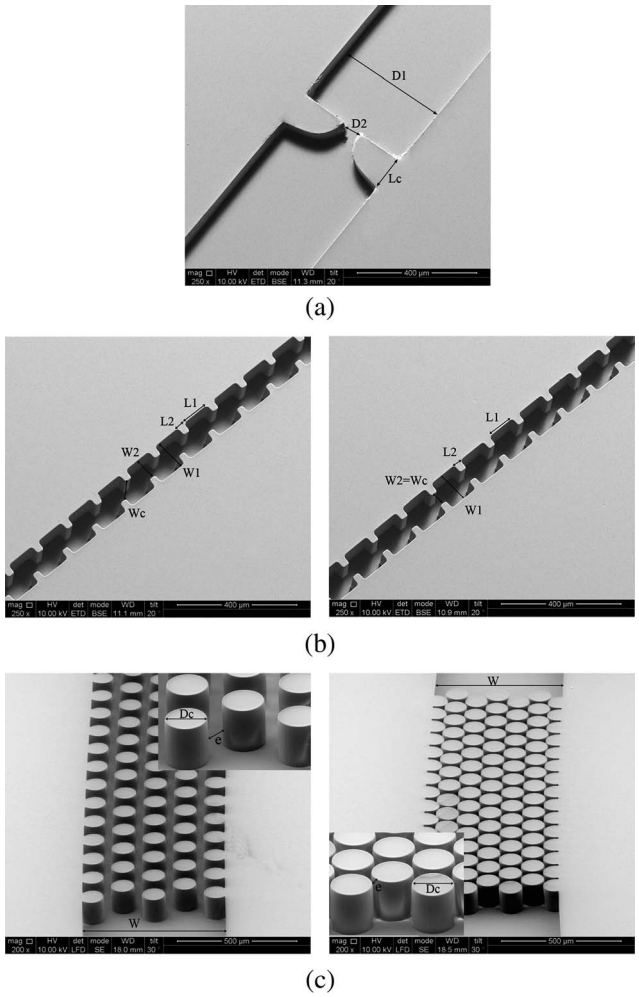

Fig. 3 SEM images of the microfluidic devices: (a) microchannel with a hyperbolic contraction–abrupt expansion; (b) microfluidic analogues of porous media in symmetric (right) and asymmetric (left) configurations; (c) microfluidic devices composed of an array of cylinders with different interstitial spacings: $e = 50$ μm (left) and $e = 10$ μm (right).

Microfluidic channels with a periodic arrangement (Fig. 3b), consisting of a continuous series of contractions and expansions with 117 repeating units (symmetric and asymmetric), were used as 1-D porous media analogues as explained in Galindo-Rosales *et al.*[6]

Finally, different microchannels with a depth of 50 μm and width of $W = 600$ μm, containing arrays of 100 μm diameter cylinders (D_c) arranged to form interstitial spaces (e) between 10 and 50 μm, similar to the average interstitial spaces in real porous media, were also used in order to evaluate the influence of interstitial spacing in the gelation process (Fig. 3c). A similar flow configuration was used at the macroscale as a 2-D analogue of porous media by Yip *et al.*[14] with relative success.

Flow visualizations were carried out using fluorescence streak photography. The optical setup consists of an inverted epi-fluorescence microscope (DMI-5000M, Leica Microsystems GmbH)

equipped with a CCD camera (DFC350 FX, Leica Microsystems GmbH), a light source (100 W mercury lamp) and a filter cube (Leica Microsystems GmbH, excitation filter BP 530–545 nm, dichroic 565 nm and barrier filter 610–675 nm). The fluids were seeded with 1 μm fluorescent tracer particles (Nile Red, Molecular Probes, Invitrogen, Ex/Em: 520/580 nm). The microgeometry containing the seeded fluid was continuously illuminated and the light reflected by the fluorescent tracer particles was imaged through the microscope objective (10×, NA = 0.25) onto the CCD array of the camera using 'long' exposure times (which were varied according to the flow rate) in order to capture the pathlines of the tracer particles.

A syringe pump (PHD2000, Harvard Apparatus) was used to inject the fluid at constant flow rate into the microchannels, using Hamilton syringes with different volumes (50 and 100 μl), connected to the microgeometries by Tygon tubing of 0.44 mm internal diameter.

2.6 Pressure drop measurements

For the experiments in the real porous media, the liquid was introduced into the column from a pressurized reservoir; the inlet pressure could be varied and was measured with a manometer (Wika Instrument Corporation, model 332.50; range 0–2.5 bar). The flow inlet was placed at the top of the column and the outlet was located at the bottom part, where the fluid was collected and weighed to measure the mass flow rate. The pressure drop measurements were carried out between two pressure taps in the column separated by a distance of $L = 14.7 \pm 0.1$ cm using differential pressure sensors (Honeywell 26PC series) covering ranges up to $\Delta P = 207$ kPa.

For the symmetric and asymmetric microchannel 1-D analogues of the porous media, the ports of the differential pressure transducers were connected to two pressure taps, located upstream and downstream of the test section, containing the 117 repeating units. A 10 V DC power supply (Lascar electronics, PSU 206) was used to power the pressure sensors that were also connected to a computer *via* a data acquisition card (NI USB-6218, National Instruments) in order to record the output data using LabView v8.2 software. The transient response of the pressure sensors was continuously recorded until steady-state was reached. To compare the results of the microchannels with the real porous media, we measured the variation of the pressure gradient as function of the interstitial velocity in both systems.[6]

3 Results and discussion

3.1 Nanogel formation

The Boger fluid flows through the real porous media were initially evaluated by flowing samples of 50 and 125 ppm of PAA with 1% of NaCl through three different porous media: sand with $x_{32} = 400$ μm and ballotini with $x_{32} = 403$ and 150 μm. Fig. 4 presents the variation of the pressure gradient across the bed, $\Delta P/L$, with the interstitial velocity, U_i. For all packed beds, the variation is linear at low U_i, as also happens for Newtonian fluids. Above a critical velocity, elastic effects set in and the slope of the $\Delta P/L$ *vs.* U_i curve increases significantly. The PAA solution of 125 ppm with salt produces higher pressure gradients than the 50 ppm sample, given the slightly higher viscosity of the former (*cf.* Fig. 1a), and also due to its higher relaxation time, which increases with the polymer concentration, thus leading to flow instabilities at lower flow rates. For the sand bed and the ballotini bed of $x_{32} = 150$ μm, larger pressure drops are observed, but above a critical pressure gradient the observed flow rate actually decreases (delimited by a rectangle in Fig. 4). This effect corresponds to a significant decrease in the permeability of the porous medium, and probably is a consequence of a gelation process of the polymer solutions subject to high shear and/or elongational strain rates. We note, however, that for the bed of ballotini with $x_{32} = 403$ μm this flow rate reduction at higher pressure gradients is not observed in the range of flow rates investigated.

The trigger of this gelation process could lie in the fact that the polymer solution adsorbs on the solid surfaces of the particles of the porous media containing silica (SiO_2).[19,20] This is supported by some experimental tests carried out by Story *et al.*[21] which showed that polyacrylamide is able to interact with sand, creating a coating layer which envelops the particles of the porous media. Furthermore, polymer adsorption kinetics increase significantly with an increase in the electrolyte concentration as reported by Al-Hashmi and Luckham[22] for the same type of non-ionic PAA as used in our work. This fact could explain the absence of gel formation when aqueous polymer solutions of PAA without salt flow through the same porous media.[6] Moreover, it is also known that the adsorption is enhanced with the increase of the molecular weight of the polymer.[23] As such, the high molecular weight of the PAA used here is prone to favour the adsorption process even more.

After this initial interaction of the PAA molecules with sand or with ballotini particles, which have a chemical composition similar to sand with a high amount of SiO_2, a jamming phenomenon occurs gradually which is enhanced at very large deformation rates. A jamming clogging effect was also observed by Srikar *et al.*[24] in homogeneous solutions of Rhodamine 610 chloride flowing through carbon micro and nanotube bundles. In our case, the gelation process is the outcome of a sequence of events, acting like a snowball effect: after the initial adsorption of the PAA molecules on the SiO_2 surfaces, the jamming phenomenon of the polymer chains occurs by a simultaneous combination of extreme shear (relatively high flow rates) and elongational conditions (narrow interstitial spacing), combined with flow induced initial aggregation of the polymer chains that contribute to decrease the effective pore size. When the jamming occurs, the polymer chains lose flexibility and, as a consequence, a blockage of the porous medium occurs. It is also important to emphasize that the addition of NaCl to the polymer solutions of PAA favours the absorption of water by the gel.[25]

Additional experiments were also carried out in the real porous medium with ballotini of particle diameter $x_{32} = 150$ μm starting at high flow rates and progressing to low flow rates, to complement those from low to high flow rates. Fig. 5 shows the results of these experiments carried out with clean ballotini particles for each test and under the same conditions. It is clear that when the flow is initially slow, favouring the adsorption of the polymer on the particles, a blockage of the porous medium is observed after the second slope of the pressure gradient curve shown in Fig. 5. However, no sign of gel formation was observed when the flow started at higher flow rates, possibly due to the

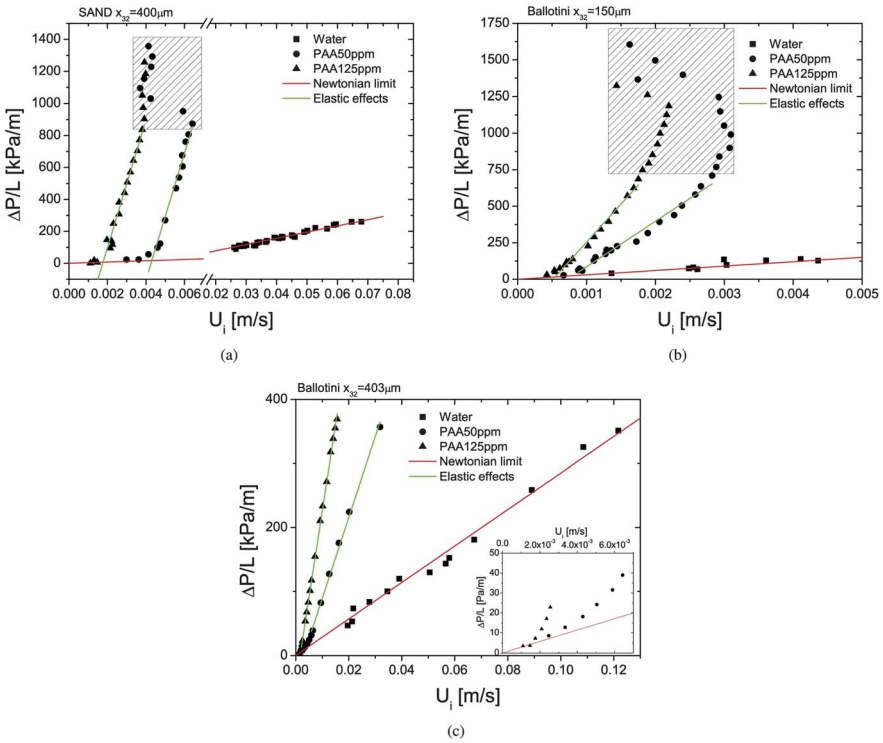

Fig. 4 Influence of interstitial velocity on the measured pressure gradient for flow through porous media consisting of (a) sand of $x_{32} = 400$ μm, and (b) ballotini of $x_{32} = 150$ and (c) 403 μm.

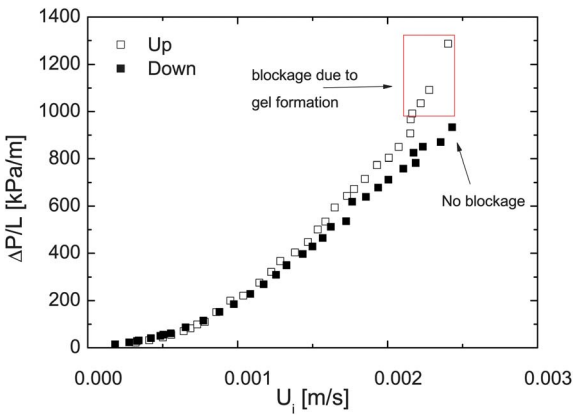

Fig. 5 Influence of interstitial velocity on the measured pressure gradient through the porous medium of ballotini of $x_{32} = 150$ μm using a 125 ppm PAA aqueous solution with 1% of NaCl. The flow rate was varied in the first experiment from low to high values (Up) and in the second experiment from high to low (Down) values.

shorter times and the larger shear stresses at the walls, which delay the initial adsorption of the PAA molecules and consequently, the jamming process at high deformation rates is inhibited. When the adsorption becomes relevant, at larger times, the corresponding lower flow rates do not favour the jamming phenomena and no blockage is observed.

3.2 Theory validation

3.2.1 Cryo-SEM analysis. In this section we focus particularly on the real porous media made of sand ($x_{32} = 400$ μm) and of ballotini ($x_{32} = 150$ μm), as no atypical behaviour was found for the porous medium of ballotini with particle diameter $x_{32} = 403$ μm.

The Cryo-SEM images clearly show a nanogel structure. Through observation of a broken portion of the porous media bed after freezing, it was possible to see a vast structure formed within the interstitial spaces in between the particles (Fig. 6). For the case of the ballotini (Fig. 6a), this structure is akin to the hydrogel structure formed when a hydrogel glue (Tissue-Tek®, Agar Scientific) is added to new ballotini particles and is subsequently observed by Cryo-SEM (Fig. 7). On the other hand, in the case of the sand (Fig. 6b), the structure seems to be less pervasive, *i.e.*, it is not covering the sand particles in such an extensive manner. This can be justified with the fact that the sand particles are on average two and a half times larger than the ballotini particles, are not spherical and exhibit a wider distribution of sizes, when compared to the ballotini particles. As a result, the porous bed in this case is highly non-homogeneous with a wide range of interstitial spacings and, as observed by SEM (Fig. 6), the gel structure seems to appear at small interstitial spaces (less than 10 μm approximately). In the case of ballotini these smaller interstices occur more frequently due to the smaller and more homogeneous particle size distribution.

3.2.2 Flow under controlled shear and extensional conditions. In order to confirm that the origin of the gelation is not just a consequence of pure shear and/or pure extensional strain rates, but also because of an adsorption phenomenon of the PAA molecules on the surface of the particles of the porous media, different shear and extensional experiments were carried out under controlled flow conditions. On the one hand, LAOS and

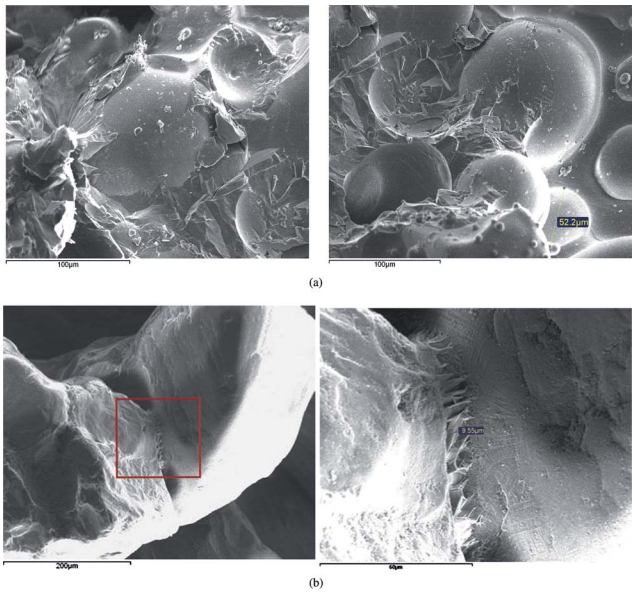

Fig. 6 Cryo-SEM images obtained with (a) ballotini of $x_{32} = 150$ μm and (b) sand with $x_{32} = 400$ μm (the image on the right corresponds to a zoomed view of the region enclosed by the red rectangle on the image on the left), after use in the experiments that lead to flow induced gelation using a solution of 125 ppm of PAA with 1% of NaCl.

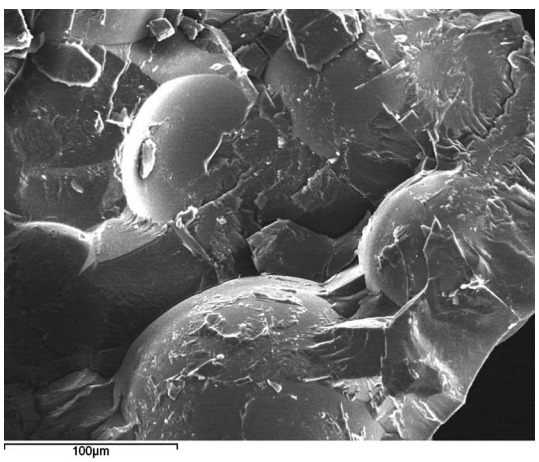

Fig. 7 Cryo-SEM image obtained using ballotini ($x_{32} = 150$ μm) covered with a hydrogel glue.

steady shear flow tests were conducted to measure the rheological properties at high shear rates; on the other hand, flow visualizations through a microscale hyperbolic contraction (which induces a quasi-uniform extensional rate flow at the centre line of the microgeometry) were done in order to understand the effects of the high extensional strain rates that can be achieved in such devices.

To assess the progressive transition from linear to nonlinear rheological response, LAOS measurements were carried out over a wide range of strain amplitudes at a constant angular frequency, $\omega = 1$ rad s^{-1}. The Lissajous diagram (Fig. 1b) shows that at high strains, samples show a viscous behaviour, since the stress is out of phase with the strain and the area enclosed presents a quasi-circular shape (a circular shape corresponds to an ideal liquid) and is larger, reflecting the predominance of the dissipated energy. This is confirmed with the stress/strain rate diagram in which the area is small, corresponding to a reduced stored energy,[16,17,26] indicating a viscous-like behaviour at high deformations.

We have also examined the flow patterns in the hyperbolic contraction/sudden expansion for the solutions with 50 and 125 ppm of PAA with 1% of NaCl. Converging entry flows show complex flow patterns combining both shear and extensionally dominated regions; near the walls shear effects dominate, while along the centre line the flow is primarily extensional and essentially shear-free. High flow rates were applied in order to induce high deformation rates. No sign of gelation was observed up to the highest flow rate used in the experiments, $Q = 100$ ml h^{-1}, corresponding to an extensional rate of $\dot{\varepsilon} \approx (U_2 - U_1)/L_c \approx 8 \times 10^5$ s^{-1}, where U_1 and U_2 are the bulk velocities in the upstream channel and at the throat of the contraction, respectively, and L_c is the contraction length (*cf.* Fig. 3a). Beyond this flow rate the resulting pressure is so high that the microchannel is damaged. We thus conclude that pure extensional strain rates in PDMS microfluidic hyperbolic contractions are not sufficient to induce the gelation of the polymer solutions.

Additionally, flow visualizations and pressure drop measurements through the microchannel analogues of the porous media were carried out to assess whether the gel formation could be due to a combination of shear and extensional deformations. The microchannels used here are identical to those used by Galindo-Rosales *et al.*,[6] which are able to mimic a porous bed with $x_{32} = 390$ μm. Pressure drop measurements of the polymer solutions through the 1-D porous media analogue channels, together with the pressure drop measurements obtained from the real porous media are compared in Fig. 8. In this case the pressure gradient is plotted as a function of the Deborah number, which is defined as:

$$De = \lambda \frac{U}{L}, \tag{1}$$

where λ is the longest relaxation time measured in the CaBER (*cf.* Section 2.2), L is a characteristic length scale (taken as the particle Sauter mean diameter in the case of the real porous media and as the equivalent particle size in the case of the microchannel 1-D analogue of the porous media) and U is a characteristic velocity (taken as the interstitial velocity). The Deborah number represents a ratio of time scales of the material (λ) and of the flow process (L/U), allowing the comparison of the results obtained in the microchannels with those obtained with the porous media.

As illustrated in Fig. 8, the pressure gradient curves measured in the 1-D porous media analogue microchannels are qualitatively different from the pressure gradient curves for the two real porous media when the formation of gel is observed, because of the absence of the third slope region in the former. It is also important to point out that the results obtained with the ballotini of $x_{32} = 403$ μm not only do not show the third slope in the pressure gradient curve, but the onset of elastic instabilities is not matched by the results obtained in the microchannels, since the latter correspond to a simplified one-dimensional model of real porous media where the elastic effects are less pronounced. The onset of the rise in the pressure gradient for the ballotini of

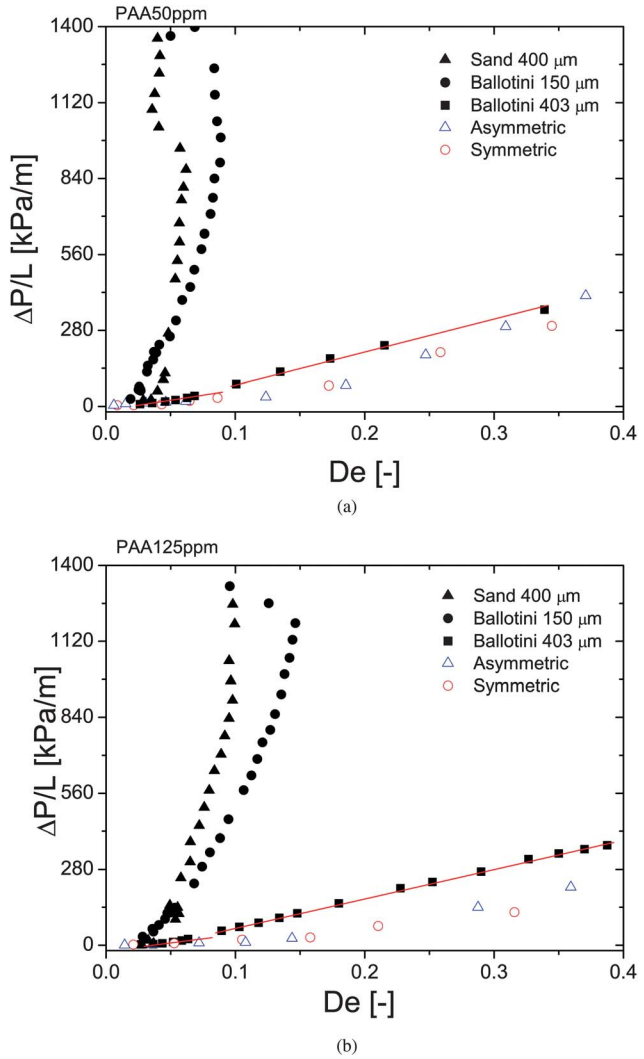

Fig. 8 Influence of the Deborah number on the measured pressure gradient through the real and the 1-D porous media analogue microchannels, for (a) 50 and (b) 125 ppm PAA aqueous solutions with 1% of NaCl.

$x_{32} = 403$ μm occurs at a Deborah number corresponding to about one third of the critical value for the microfluidic devices. Therefore, flow visualizations and pressure gradient measurements of the fluid flow through the asymmetric and symmetric configurations did not provide new insights about the gelation phenomenon observed in the real porous media. The absence of gel formation in the microchannel 1-D porous media analogues, even when the Boger fluid flow in the microchannels occurs at similar interstitial velocities as in the real porous media, is consistent with the lack of strong interactions between PAA and PDMS that preclude the gelation process. However, one may argue that the flow paths in the analogues are not so meandering as in the real porous media. Therefore, in order to clarify this issue, the Boger fluid flows were also investigated using microchannels with an array of cylinders. Two different configurations were used, one with an interstitial space of 50 μm and another with 10 μm. In both cases the length of the cylinders is 50 μm (same as the depth of the microchannel). These configurations are used in order to ensure that shear and extensional effects are relevant in the flow inside the microchannels. Fig. 9 shows that for the microdevice of 50 μm of interstitial space, no signs of gelation were observed, for flow rates from 0.1 ml h^{-1} to 0.24 ml h^{-1}. The same result was obtained for the microchannels with 10 μm of interstitial spacing. In this case the flow rates were varied from 0.01 ml h^{-1} to 0.9 ml h^{-1} in order to obtain interstitial velocities up to and above the conditions where the blockage due to gelation was observed in the real porous media. No evidence of gel formation was observed in the microdevices made of PDMS, even when the interstitial spacing was of the same order of that found in the real porous media. As seen in Fig. 9 there is no evidence of flow induced gelation. We can observe, however, elastic-driven flow instabilities.

3.2.3 Flow through plastic bead porous media. In order to corroborate the importance of the adsorption phenomenon of the PAA molecules on the surface of particles containing silica in the gelation process, different experiments were carried out in the real porous media using two sizes of plastic spheres ($x_{32} = 142$ μm and 81 μm) without any trace of SiO_2 in their composition.

The porous medium made of plastic particles of $x_{32} = 142$ μm, has nearly the same interstitial spacing as the ballotini porous medium with $x_{32} = 150$ μm, but no third slope is observed in the pressure gradient flow curve for both samples of 125 and 50 ppm of PAA with 1% of NaCl (Fig. 10), and therefore no gelation is found. The experimental conditions are the same as those in the case of ballotini with $x_{32} = 150$ μm and sand particles with $x_{32} =$ 400 μm, apart from the fact that the plastic spheres do not

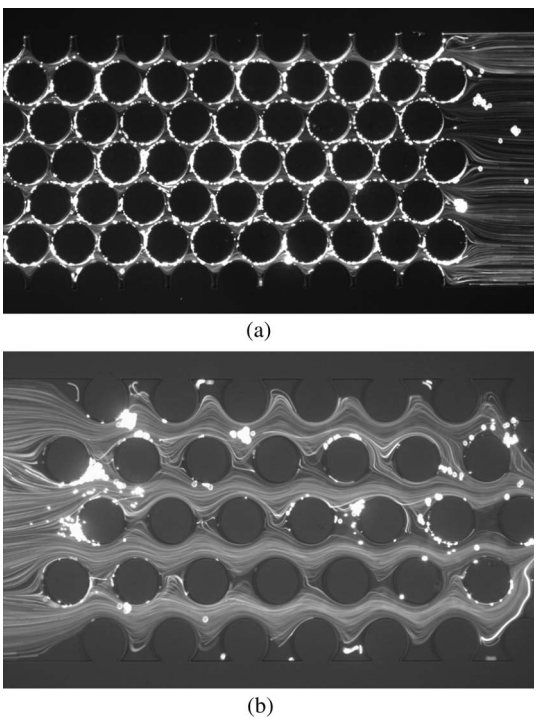

Fig. 9 Flow visualization in the microchannels with cylinder arrays; (a) cylinders with interstitial spacing of 10 μm ($Q = 0.6$ ml h^{-1}); (b) cylinders with interstitial spacing of 50 μm ($Q = 0.2$ ml h^{-1}), using an aqueous solution of PAA with 50 ppm with 1% of NaCl.

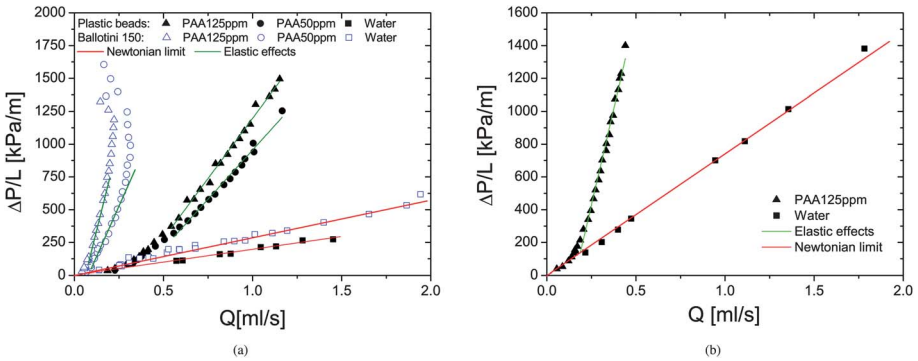

Fig. 10 Influence of the flow rate on the measured pressure gradient through the porous media made of plastic beads of (a) $x_{32} = 142$ μm and (b) 81 μm for water and PAA aqueous solutions of 50 and 125 ppm with 1% of NaCl. The results obtained with ballotini of $x_{32} = 150$ μm are shown in (a) for comparison purposes.

contain any trace of silica. If we take the conditons to further extremes, by decreasing the interstitial spacing using 81 μm diameter plastic beads, while working with the fluid with the highest polymer concentration (125 ppm), our results again confirm the absence of gelation, as shown in Fig. 10b. In this way we confirm that the gelation process starts at high deformation rates, but only when an initial adsorption phenomenon of PAA molecules occurs at the surface of the particles containing SiO_2.

4 Concluding remarks

In this work we describe several experiments that were carried out in order to explain a flow-induced gelation phenomenon of low viscosity dilute aqueous solutions of PAA containing 1% of NaCl when they flow through unconsolidated sand and ballotini beds. This involved an extensive investigation of the flows of such fluids in various geometries including standard rheological flows, hyperbolic contractions, meandering channels and arrays of cylinders, as well as the effect of different materials. The results suggest that the gelation process starts with the adsorption of PAA molecules on the surface of the particles, but only takes place for those containing a high fraction of silica (here sand and ballotini). Additionally it is necessary to achieve extreme shear and elongational flow conditions, and interstitial spaces smaller than about 10 μm. Following the adsorption, a jamming process takes place at high deformation rates leading to gel formation and blockage of the porous media.

Acknowledgements

Authors acknowledge funding from Fundação para a Ciência e a Tecnologia (FCT), COMPETE and FEDER through projects PTDC/EME-MFE/99109/2008, PTDC/EME-MFE/114322/2009, REEQ/928/EME/2005, REEQ/262/EME/2005 and scholarships SFRH/BPD/69663/2010 and SFRH/BPD/69664/2010.

References

1 V. Berejnov, N. Djilali and D. Sinton, Lab-on-chip methodologies for the study of transport in porous media: energy applications, *Lab Chip*, 2008, **8**, 689–693.
2 W. Kozicki, Viscoelastic flow in packed beds or porous media, *Canadian Journal of Chemical Engineering*, 2001, **79**, 124–131.
3 B. K. Rao, Internal heat transfer to viscoelastic flows through porous media, *Exp. Heat Transfer*, 2000, **13**, 329–345.
4 J. Niu, C. Fu and W. C. Tan, Thermal convection of a viscoelastic fluid in an open-top porous layer heated from below, *J. Non-Newtonian Fluid Mech.*, 2010, **165**, 203–211.
5 T. Sochi, Non-Newtonian flow in porous media, *Polymer*, 2010, **51**, 5007–5023.
6 F. J. Galindo-Rosales, L. Campo-Deaño, M. S. N. Oliveira, M. A. Alves, F. T. Pinho, E. V. Bokhorst and P. J. Hamersma, Microfluidic systems for the analysis of viscoelastic flow phenomena occurring in porous media, *Microfluid. Nanofluid.*, 2012, **12**, 485–498.
7 N. Y. Gaitonde and S. Middleman, Flow of viscoelastic fluids through porous media, *Ind. Eng. Chem. Fundam.*, 1966, **6**, 145–147.
8 E. H. Wissler, Viscoelastic effects in the flow of non-Newtonian fluids through a porous medium, *Ind. Eng. Chem. Fundam.*, 1971, **10**, 411–417.
9 A. Aitkadi, P. Carreau and G. Chauveteau, Rheological properties of partially hydrolyzed polyacrylamide solutions, *J. Rheol.*, 1987, **31**, 537–561.
10 J. R. Stokes, L. J. W. Graham, N. J. Lawson and D. V. Boger, Swirling flow of viscoelastic fluids. Part 1. Interaction between inertia and elasticity, *J. Fluid Mech.*, 2001, **429**, 67–115.
11 J. R. Stokes, L. J. W. Graham, N. J. Lawson and D. V. Boger, Swirling flow of viscoelastic fluids. Part 2. Elastic effects, *J. Fluid Mech.*, 2001, **429**, 117–153.
12 L. Campo-Deaño, F. J. Galindo-Rosales, F. T. Pinho, M. A. Alves and M. S. N. Oliveira, Flow of low viscosity Boger fluids through a microfluidic hyperbolic contraction, *J. Non-Newtonian Fluid Mech.*, 2011, **166**, 1286–1296.
13 B. Khomami and L. D. Moreno, Stability of viscoelastic flow around periodic arrays of cylinders, *Rheologica Acta*, 1997, **36**, 367–383.
14 R. Yip, D. F. James and I. G. Currie, PIV measurements of slow flow of a viscoelastic fluid within a porous medium, *Exp. Fluids*, 2011, **51**, 801–809.
15 M. Vasudevan, E. Buse, D. Lu, H. Krishna, R. Kalyanaraman, A. Q. Shen, B. Khomami and R. Sureshkumar, Irreversible nanogel formation in surfactant solutions by microporous flow, *Nat. Mater.*, 2010, **9**, 436–441.
16 R. Ewoldt, A. E. Hosoi and G. H. McKinley, New measures for characterizing nonlinear viscoelasticity in large amplitude oscillatory shear, *J. Rheol.*, 2008, **52**, 1427–1458.
17 J. Lauger and H. Stettin, Differences between stress and strain control in the non-linear behavior of complex fluids, *Rheol. Acta*, 2010, **49**, 909–930.
18 M. S. N. Oliveira, L. E. Rodd, G. H. McKinley and M. A. Alves, Simulations of extensional flow in microrheometric devices, *Microfluid. Nanofluid.*, 2008, **5**, 809–826.
19 X. Song, J. Ke, B. Han, G. Yang and H. Yan, Enthalpy of adsorption and adsorption isotherms of polyacrylamide on sea sand, *J. Therm. Anal.*, 1995, **45**, 7–12.
20 M. Wisniewska, The temperature effect on the adsorption mechanism of polyacrylamide on the silica surface and its stability, *Appl. Surf. Sci.*, 2012, **258**, 3094–3101.

21 B. Story, M. A. Urynowicz, D. Johnson and J. Morris, Infiltration effects of polyacrylamide adsorption on porous media, *ASCE Conf. Proc*, 2007, **243**, 157.
22 A. R. Al-Hashmi and P. F. Luckham, Characterization of the adsorption of high molecular weight non-ionic and cationic polyacrylamide on glass from aqueous solutions using modified atomic force microscopy, *Colloids Surf., A*, 2010, **358**, 142–148.
23 K. Holmberg, B. Jonsson, B. Kronberg and B. Lindman, *Surfactants and Polymers in Aqueous Solution*, John Wiley & Sons, Ltd., 2002, ch. 19, pp. 404–407.
24 R. Srikar, A. L. Yarin and C. M. Megaridis, Fluidic delivery of homogeneous solutions through carbon tube bundles, *Nanotechnology*, 2009, **20**, 275706.
25 J. Thiel and G. Maurer, Swelling equilibrium of poly(acrylamide) gels in aqueous salt and polymer solutions, *Fluid Phase Equilib.*, 1999, **165**, 225–260.
26 K. Hyun, M. Wilhelm, C. O. Klein, K. S. Cho, J. G. Nam, K. H. Ahn, S. J. Lee, R. H. Ewoldt and G. H. McKinley, A review of nonlinear oscillatory shear tests: Analysis and application of large amplitude oscillatory shear (LAOS), *Prog. Polym. Sci.*, 2011, **36**, 1697–1753.

Addition and correction

Note from RSC Publishing

This article was originally published with incorrect page numbers. This is the corrected, final version.

The Royal Society of Chemistry apologises for these errors and any consequent inconvenience to authors and readers.